JOURNAL OF TISSUE ENGINEERING AND REGENERATIVE MEDICINE
J Tissue Eng Regen Med (2015)
Published online in Wiley Online Library (wileyonlinelibrary.com) **DOI:** 10.1002/term.2017

RESEARCH ARTICLE

Characterization and biocompatibility of a fibrous glassy scaffold

P. R. Gabbai-Armelin[1,4], M. T. Souza[2], H. W. Kido[1,4], C. R. Tim[1,4], P. S. Bossini[3], K. R. Fernandes[3], A. M. P. Magri[3], N. A. Parizotto[4], K. P. S. Fernandes[5], R. A. Mesquista-Ferrari[5], D. A. Ribeiro[3], E. D. Zanotto[2], O. Peitl-Filho[2] and A. C. M. Renno[3]*

[1]*Post-Graduate Programme of Biotechnology, Federal University of São Carlos (UFSCar), SP, Brazil*
[2]*Vitreous Materials Laboratory (LaMaV), Department of Materials Engineering, Federal University of São Carlos (UFSCar), SP, Brazil*
[3]*Department of Biosciences, Federal University of São Paulo (UNIFESP), Santos, SP, Brazil*
[4]*Department of Physiotherapy, Federal University of São Carlos (UFSCar), SP, Brazil*
[5]*Department of Rehabilitation Sciences and Biophotonics Applied to Health Sciences, Nove de Julho University (UNINOVE), São Paulo, SP, Brazil*

Abstract

Bioactive glasses (BGs) are known for their ability to bond to living bone and cartilage. In general, they are readily available in powder and monolithic forms, which are not ideal for the optimal filling of bone defects with irregular shapes. In this context, the development of BG-based scaffolds containing flexible fibres is a relevant approach to improve the performance of BGs. This study is aimed at characterizing a new, highly porous, fibrous glassy scaffold and evaluating its *in vitro* and *in vivo* biocompatibility. The developed scaffolds were characterized in terms of porosity, mineralization and morphological features. Additionally, fibroblast and osteoblast cells were seeded in contact with extracts of the scaffolds to assess cell proliferation and genotoxicity after 24, 72 and 144 h. Finally, scaffolds were placed subcutaneously in rats for 15, 30 and 60 days. The scaffolds presented interconnected porous structures, and the precursor bioglass could mineralize a hydroxyapatite (HCA) layer in simulated body fluid (SBF) after only 12 h. The biomaterial elicited increased fibroblast and osteoblast cell proliferation, and no DNA damage was observed. The *in vivo* experiment showed degradation of the biomaterial over time, with soft tissue ingrowth into the degraded area and the presence of multinucleated giant cells around the implant. At day 60, the scaffolds were almost completely degraded and an organized granulation tissue filled the area. The results highlight the potential of this fibrous, glassy material for bone regeneration, due to its bioactive properties, non-cytotoxicity and biocompatibility. Future investigations should focus on translating these findings to orthotopic applications. Copyright © 2015 John Wiley & Sons, Ltd.

Received 21 May 2014; Revised 16 December 2014; Accepted 15 January 2015

Keywords **biocompatibility; biomaterial; bioactive glass; fibrous scaffold; bone repair; cytotoxicity**

1. Introduction

Bone fractures occur daily worldwide, with 6.2 million cases/year being reported in the USA alone (Claes and Willie, 2007). Among these, 5–10% showed delayed healing, with some persisting for > 9 months or even resulting in non-union fractures. Multiple factors can impair fracture consolidation, including significant bone loss caused by diseases, trauma or tumour resection (Gautier and Sommer, 2003). To ensure the proper repair of the skeleton and decrease the chances of complications from abnormal bone repair, the development of strategies based on the mechanisms of the fracture-healing process is required (Gautier and Sommer, 2003).

Biomaterials that can induce bone biomineralization have been in high demand for clinical regenerative medicine and tissue engineering (Hench, 2006). They combine a number of materials of natural or synthetic origins that

*Correspondence to: Ana C. M. Renno, Department of Biosciences, Federal University of São Paulo (UNIFESP), Avenida Ana Costa 95, Santos, SP 11050-240, Brazil. E-mail: a.renno@unifesp.br

have the capacity to chemically adhere to bone tissue (Hubbell, 1998; Hench and Polak, 2002).

Bioactive glasses (BGs) have been widely used to improve bone healing and accelerate bone metabolism (Hench, 2006). The most-known bioactive glass is Bioglass® 45S5, which presents the highest bioactivity index so far reported. It is a silica-based melt or gel-derived glass characterized by a SiO_2 content of $< 60\%$, high Na_2O and CaO contents and a high $CaO{:}P_2O_5$ ratio. Many studies have shown that Bioglass 45S5 stimulates *in vitro* osteogenesis, inducing the proliferation of human osteoblasts, and accelerates bone consolidation in animal experimental models (Xynos *et al.,* 2000; Xie *et al.,* 2009; Granito *et al.,* 2011). Additionally, the angiogenic potential of Bioglass 45S5 has been demonstrated (Day *et al.,* 2005; Gorustovich *et al.,* 2010).

In general, bioactive glasses are primarily available as powders and monoliths. One of the main disadvantages of those forms is that an optimal filling of irregularly shaped bone defects is extremely difficult (Day *et al.,* 2005; Vallet-Regi, 2006). Additionally, the lack of interconnected pores in the implants limits inner cell ingrowth. To overcome these limitations, the interest in alternative products, such as malleable/fibrous porous implants and BG-based scaffolds, has increased (Chen *et al.,* 2006; Rahaman *et al.,* 2011; Jones, 2013; Lacroix *et al.,* 2014). These products are particularly interesting because they are more suitable fillers for different sizes or forms of bone defect and present an interconnected porous structure (Moimas *et al.,* 2006; Brown *et al.,* 2008).

In view of the growing interest in the development of more efficient materials to be used as bone grafts, it is hypothesized that the development of a brand new, porous, fibrous glassy scaffold belonging to the SiO_2–Na_2O–K_2O–MgO–CaO–P_2O_5 system might offer a novel way of improving the biological performance of BGs.

The new fibrous biomaterial aims to integrate high porosity with high bioactivity, which is typical of BGs, to increase the application range of the material. Despite these possible advantages, before this biomaterial can be used clinically, it is necessary to investigate its physicochemical characteristics and subsequent biological responses. Consequently, the aim of the current study was to investigate the morphological features and the *in vitro* and *in vivo* biocompatibilities of the new, fibrous glassy scaffolds. To this end, the precursor bioactive glass was evaluated by *in vitro* studies with SBF-K9 solution, and the manufactured scaffolds were analysed by scanning electron microscopy (SEM), pH measurements and mass loss quantification. In addition, the biocompatibility was evaluated by *in vitro* (i.e. indirect cell proliferation and evaluation of DNA damage) and *in vivo* (i.e. subcutaneous implantation) studies. For this purpose, MTT and comet assays were performed in fibroblast and osteoblast cells, which were seeded in contact with biomaterial extracts after 24, 72 and 144 h. Also, scaffolds were implanted subcutaneously in rats for histocompatibility evaluation 15, 30 and 60 days after implantation.

2. Materials and methods

2.1. Material preparation

The fibrous glassy scaffolds were manufactured using fibres obtained from a new bioactive glass composition of the SiO_2–Na_2O–K_2O–MgO–CaO–P_2O_5 system (Souza *et al.,* 2013). The bioactive glass was prepared and homogenized in a platinum crucible by thoroughly mixing and melting the chemical reagents at 1200°C (crushing and remelting at 1200°C five additional times). After the production of the glass, bioactive fibres were drawn in a homemade fibre tower. This new composition was developed with the specific aim of producing fibres, because the traditional 45S5 glass is not able to be drawn into fibres.

After this procedure, highly porous circular scaffolds (10 x 2 mm^2) were obtained using chopped fibres (3 mm length) at room temperature. The fibre fragments were weighed and randomly placed in a cylindrical polytetrafluoroethylene mould to obtain a disc-shaped sample, using moderate compression stress.

The morphology of the scaffolds was analysed using a scanning electron microscope (LEO 440, LEO Electron Microscopy).

2.2. Characterization of the fibrous glassy scaffold

2.2.1. Porosity measurements

To measure their porosity, the scaffolds were immersed in epoxy-resin under vacuum and, after hardening, they were polished from 200 to 1200 grit, sputter-coated with gold and examined by SEM (Phenom™, FEI Co.) (Karageorgiou and Kaplan, 2005; Ghasemi-Mobarakeh *et al.,* 2007; Narayan, 2009; Mirhadi, 2014). The glass:epoxy area ratio was measured using ImageJ 1.46r software, using 15 representative photographic images to determine the mean porosity of the scaffolds.

2.2.2. Mineralization evaluation

In vitro tests using simulated body fluid K9 (SBF-K9) solution were conducted, using the methodology of Kokubo *et al.* (1990) to verify the bioactivity of this new glass composition and evaluate the degradation rate and formation of HCA layer. Briefly, glass samples were cut into cylinders of approximately 2 mm height × 12 mm diameter and then polished with 400-grit silicon carbide paper. All samples were rinsed and cleaned with isopropyl alcohol solution in an ultrasonic cleaner for 20 min. Then the samples were immersed in SBF-K9 solution and placed into a sealed polyethylene bottle with a glass surface area:volume ratio of 0.1 cm^{-1}. The HCA layer formation was analysed by Fourier transform infrared spectroscopy

DOI: 10.1002/term

(FTIR; Perkin-Elmer, Spectrum GX, DE) after periods of 4, 8, 12 and 16 h.

2.2.3. pH measurements and mass loss quantification

For the pH and mass loss evaluations, the scaffolds were placed in 3 ml phosphate-buffered saline (PBS; 10 mM, pH 7.4) and incubated at 37°C in a water bath on a shaker table (70 rpm) for 1, 7 and 14 days. The assays were performed in triplicate ($n = 3$). After the experimental periods, the scaffolds were removed from the solution and subjected to analysis.

2.2.3.1. pH measurements. Directly after the removal of the scaffolds from the water bath, the pH of the PBS medium was measured (Meterlab PHM210, calibrated with IUPAC buffers S11M002, S11M004, S11M007 from Radiometer Analytical, Villeurbanne, France).

2.2.3.2. Mass loss quantification. At each time point, the scaffolds were removed from the solution and vacuum-dried overnight before measuring the mass. The mass loss of a sample was calculated using the following formula:

$$\text{Mass loss}\ (\%) = [(W_t - W_0)/W_0] \times 100\%$$

where W_0 is the weight of the sample before immersion in PBS and W_t is the weight of the sample after immersion in PBS.

2.3. *In vitro* study

2.3.1. Cell culture

In the *in vitro* study, L929 (murine fibroblasts) and OSTEO-1 (neonatal murine calvarial osteoblastic) cells were used for cytotoxicity and genotoxicity studies. These cell lineages were selected because of their close contact to the fibrous scaffold in ectopic and orthotopic applications of the biomaterial. Additionally, L929 lineages are widely used for biocompatibility tests (Serrano *et al.,* 2008; Nath *et al.,* 2010; Liu and Chang, 2012; Kido *et al.,* 2013).

Both cell types were cultured in Dulbecco's modified Eagle's medium (DMEM; Vitrocell, Campinas, SP, Brazil) supplemented with 10% fetal bovine serum (FBS; Vitrocell) and 1% antibiotic–antimycotic solution (Vitrocell) at 37°C in a humidified atmosphere of 5% CO_2. Cells were maintained at subconfluent densities and subcultured every 2–3 days until use.

2.3.2. Cytotoxicity analysis

In the cytotoxicity analysis, an indirect assay (MTT) was used to measure the effects on cell viability of the products leached from the fibrous glassy scaffolds (Mosmann, 1983) according to Kido *et al.* (2013). L929 and OSTEO-1 cells were divided into a control group (CG) and a biomaterial group (BG). In the CG, only DMEM was used to culture the cells, whereas in the BG the cells were grown with fibrous glassy scaffold extracts. These extracts were obtained by immersing and incubating the scaffolds in supplemented DMEM at 37°C for 7 days; this DMEM was considered to be 100% concentrated with the extracts. From this primer solution, different dilutions were obtained (50%, 25% and 12.5%) (Liu *et al.,* 2009). This procedure was used to evaluate the influence on the cell proliferation of different ion concentrations leached from the biomaterial. CG and BG cells were cultured at 1×10^3 cells/well (96-well plates) for periods of 24, 72 and 144 h.

After finishing each time point, the culture plate wells were washed, using PBS, and 50 μl MTT solution (0.5 mg/ml; Sigma-Aldrich, St. Louis, MO, USA) was added to each well, then the cells were incubated in 5% CO_2 at 37°C for 3 h. Subsequently, each well received 100 μl isopropanol to dissolve the formazan crystals. A microplate (Anthos 2020, Anthos Labtec Instruments, Wals, Austria) was used to measure the absorbance reader at 620 nm. Three independent measurements were taken in quadruplicate.

2.3.3. Genotoxicity analysis

The potential damage to the DNA of fibroblastic and osteoblastic cells, which were grown with the extract of the fibrous glassy scaffold, was evaluated through an electrophoresis test in a single-cell gel, i.e. a comet assay (Tice *et al.,* 2000). This test was necessary to guarantee the safety of this new biomaterial for using as bone graft in further investigations. It is worth mentioning that genotoxicity studies are also part of (ISO IOFS, 2003) and have achieved general acceptance as serious and useful indicators of carcinogenicity (Naghavi *et al.,* 2014). For this purpose, 2×10^4 cells were added to each well of a 12-well plate. The cells were immersed in 2 ml supplemented DMEM. Fibroblastic and osteoblastic cell lines were distributed in two groups (CG and BG) and were assessed at 24, 72, and 144 h. The CG cells were cultured in supplemented DMEM without any treatment, whereas the BG cells were cultured with fibrous glassy scaffold (one scaffold/well) which was previously incubated in DMEM for 7 days (1 scaffold/2 ml medium). This assay was performed in triplicate. As the experimental periods were reached, the culture plate wells were washed with PBS, trypsinized, and the cells were placed into a 50 ml flask. The flasks were centrifuged for 5 min at 1200 rpm. Subsequently, the DMEM was removed and the cells received 1 ml fresh DMEM. After this procedure, 100 μl DMEM was added to 120 μl 0.5% low melting-point agarose (Invitrogen, New York, USA) at 37°C. The material was gently placed onto a 1.5% agarose-precoated slide and covered with a coverslip. After agarose solidification inside the refrigerator, the coverslip was removed and the slides were immersed for approximately 1 h in lysis solution [2.5 M NaCl, 100 mM EDTA (Merck, St. Louis), 10 mM Tris–HCl buffer, pH 10 (Sigma-Aldrich), 1% sodium sarcosinate (Sigma-Aldrich), with 1% Triton X-100 (Sigma-Aldrich) and 10% dimethyl

DOI: 10.1002/term

sulphoxide (Merck)]. Prior to the electrophoresis, the slides were soaked in alkaline buffer [0.3 mM NaOH (Merck) and 1 mM EDTA, pH > 13 (Merck)] for 20 min. The electrophoresis was performed at 25 V (0.86 V/cm) and 300 mA for 20 min. After this procedure, the slides were neutralized in 0.4 M Tris–HCl, pH 7.5, fixed in 100% ethanol (Merck, Darmstadt, Germany) and stained with 100 μl ethidium bromide (50 mg/ml). Ultraviolet radiation and reduced room lights were used at every step to reduce external DNA damage. The examination of 50 comets/treatment/period was performed at a magnification of ×400. This examination was captured with a black and white camera mounted on a fluorescence microscope (Olympus, Orangeburg, USA) and connected to image analysis software (Comet Assay II, Perceptive Instruments, Haverhill, Suffolk, UK). To measure the DNA damage, the tail moment was calculated; the comet tail moment is given by the product of the tail length and the fraction of DNA in the comet tail, and is positively associated with the level of DNA damage in the cell. The tail moment mean value in a specific sample was assumed to be the index of DNA damage.

2.4. *In vivo* study

2.4.1. Experimental design and surgical procedure

In the *in vivo* investigation, 30 healthy young adult male Wistar rats (age 12 weeks, weight 295 ± 29 g) were used. This study was approved by the Animal Care Committee guidelines of the Federal University of São Carlos (Protocol No. 043/2012) and the Guiding Principles for the Care and Use of Laboratory Animals were observed. All animals received one implant, placed subcutaneously into the dorsal area, to evaluate the histopathological characteristics of this fibrous glassy scaffold.

Anaesthesia was induced and maintained by isoflurane inhalation (Rhodia Organique Fine Ltd) and, to minimize post-operative discomfort, buprenorfine (Temgesic; Reckitt Benckiser Health Care Ltd, Schering-Plough, Hoddesdon, UK) was administered intraperitoneally (0.02 mg/kg) immediately after the operation and subcutaneously in the 2 days following surgery.

To insert the subcutaneous implants, the rats were immobilized on their dorsal regions and the skin was shaved and disinfected with iodine. A 2 cm incision was made in the median sagittal line, 8 cm from the skull, and a subcutaneous pocket was created by blunt dissection. The implants were randomly placed (n = 1/animal) and the skin was sutured with resorbable Vicryl® 5-0 (Johnson & Johnson, St.Stevens-Woluwe, Belgium).

The animals were housed in pairs and maintained at 24 ± 2°C, with light–dark periods of 12 h and free access to water and food. In the initial postoperative period, the intake of water and food was monitored. Furthermore, the animals were observed for signs of pain, infection and activity. After 15, 30 and 60 days post-surgery, the animals were sacrificed by CO_2 asphyxiation and the biomaterials and the surrounding tissues were harvested for histopathological analyses.

2.4.2. Histological procedures

After the subcutaneous implants had been harvested, all samples were fixed in 10% buffered formalin (Merck, Darmstadt, Germany) for 24 h. Then, the samples were dehydrated in a graded series of ethanols and embedded in paraffin. After polymerization, the specimens were submitted to histological analysis. Thin sections (6 μm) perpendicular to the longitudinal axis of the implants were prepared, using a microtome (Leica Microsystems SP 1600, Nussloch, Germany). At least two sections of each specimen were stained with haematoxylin and eosin (H&E; Merck).

2.4.3. Histological evaluation

The qualitative and quantitative histological evaluations were performed under an optical microscope (Olympus Optical Co. Ltd, Tokyo, Japan). In the qualitative analysis, the tissue response to each subcutaneous implant was assessed by evaluating inflammation, granulation tissue, and the presence of the biomaterial. Concerning the quantitative analysis, a histological grading scale, established by Jansen *et al.* (1994) and later used by Link *et al.* (2008) and Renno *et al.* (2013), was used to evaluate the capsule thickness, the tissue response of the capsule surrounding the subcutaneous implant, and also the tissue directly adjacent to the implant surface. These evaluations were performed in four predetermined fields of at least two sections of each specimen (Jansen *et al.,* 1994; Link *et al.,* 2008; Renno *et al.,* 2013). Two experienced observers (PA and HK) performed the scoring (Table 1) in a blinded manner.

2.5. Statistical analysis

Statistical data were expressed as mean and standard error (SE) of the mean values for each sample. The software utilized for this purpose was Statistica 7.0. The statistical comparisons were performed using one-way analysis of variance (ANOVA) with Tukey multiple comparison post-test. Differences were considered significant at $p \leq 0.05$.

3. Results

3.1. Characterization of the fibrous glassy scaffold

Figure 1(a) presents an overview of the fibrous glassy scaffold, which reveals that the fibres were displayed in a random way. Moreover, the SEM images at higher magnifications (×500 and ×1000; Figures 1B and C, respectively) demonstrated that the fibrous glassy scaffold was formed by interconnected porous structures.

DOI: 10.1002/term

Table 1. Histological grading scale for soft tissues

Evaluation	Response	Score
Capsule thickness	1–4 cell layers	4
	5–9 cell layers	3
	10–30 cell layers	2
	>30 cell layers	1
	Not applicable	0
Tissue response of the capsule surrounding the implants	Fibrous, mature, not dense, resembling connective or fat tissue in the non-injured regions	4
	Fibrous, but immature, showing fibroblasts and little collagen	3
	Granulous and dense, containing both fibroblasts and many inflammatory cells	2
	Consists of masses of inflammatory cells with little or no signs of connective tissue organization	1
	Cannot be evaluated because of infection or factors not necessarily related to the material	0
Tissue response directly adjacent to the implant surface (interface)	Fibroblasts contact the implant surface without the presence of macrophages or foreign body giant cells	4
	Scattered foci of macrophages and foreign body cells are present	3
	One layer of macrophages and foreign body cells is present	2
	Multiple layers of macrophages and foreign body cells are present	1
	Cannot be evaluated because of infection or other factors not necessarily related to the material	0

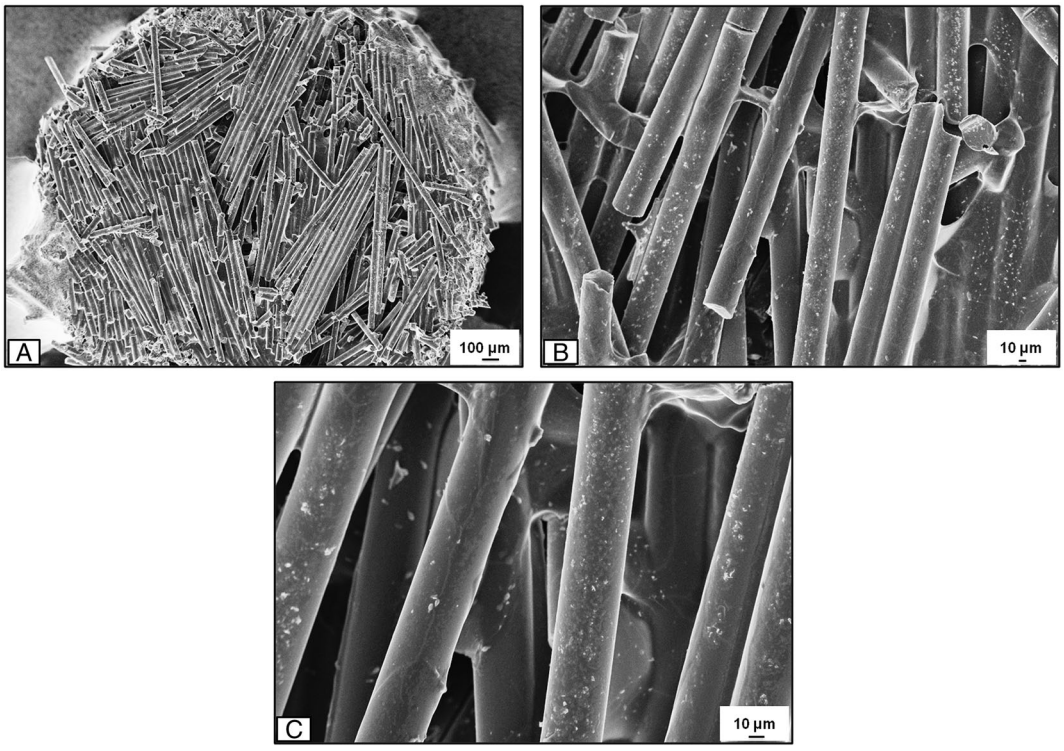

Figure 1. SEM images of the fibrous glassy scaffold: (A) overview; magnification = ×100; (B, C) higher magnifications, ×500 and ×1000, respectively

3.1.1. Porosity measurements

The evaluation of porosity (via SEM) demonstrated a total porosity of 75 ± 0.7%, with pores sizes up to 2 mm. In addition, the bioactive fibres presented diameters of approximately 45 μm (Figure 1).

3.1.2. Mineralization evaluation

The infrared spectra of a newly formed bioactive glass surface, between 0 and 16 h, are presented in Figure 2. After 12 h, peaks between 540 and 415 cm^{-1} (Si–O–Si) were no longer detected, indicating that the silica-rich layer polymerized. The presence of two peaks at approximately 610 and 560 cm^{-1} indicated that the HCA layer was formed and crystallized after only 12 h of soaking in SBF-K9 solution. These peaks became sharper and more intense over the immersion time, demonstrating the growth of crystalline apatite *in vitro*. For morphological analysis of the HCA layer, SEM images were obtained after 16 h of immersion (Figure 3); this image clearly shows the formation of the HCA layer on the glass surface. It is possible to observe the globular shape pattern that is commonly found after the precipitation and crystallization of HCA.

3.1.3. pH measurements

The results of the pH measurements during degradation are presented in Figure 4. The medium of the pre-set

DOI: 10.1002/term

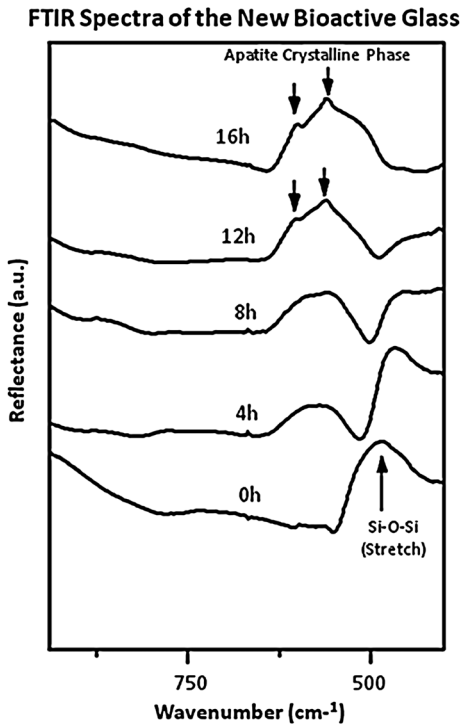

Figure 2. FTIR spectra of the new bioactive glass composition; samples in bulk form

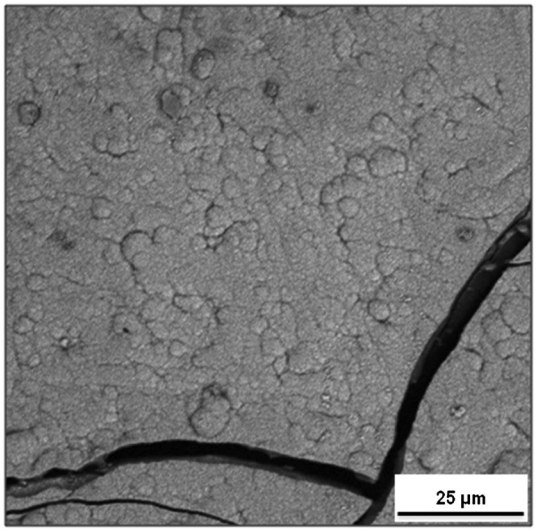

Figure 3. SEM image of HCA layer on the glass surface after 16 h of immersion in SBF; note the globular shape of the precipitated HCA; magnification = ×2300

samples showed a substantial pH increase, reaching approximately 10 and 11 on days 1 and 7 of incubation, respectively. Furthermore, the pH significantly increased to 12 on day 14 of immersion ($p < 0.05$).

3.1.4. Mass loss quantification

The mass loss evaluation showed similar results when comparing the baseline measurements with the values found after 1 and 7 days of incubation ($p > 0.05$). On

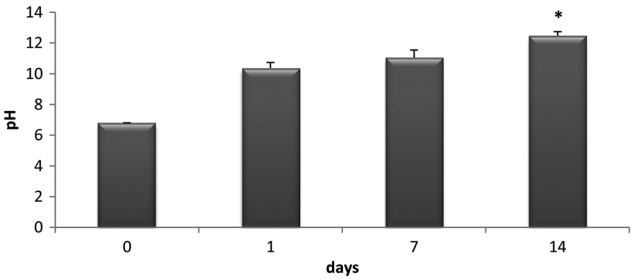

Figure 4. pH measurements of PBS after contact with fibrous glassy scaffold; *$p \leq 0.05$ vs 0, 1 and 7 days

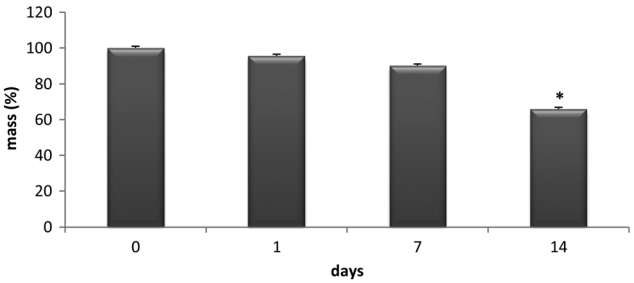

Figure 5. Mass loss of the fibrous glassy scaffold immersed in PBS for up to 14 days; *$p \leq 0.05$ vs 0, 1 and 7 days

day 14, the mass loss significantly decreased compared with the other periods ($p < 0.05$) (Figure 5).

3.2. *In vitro* results

3.2.1. Cytotoxicity analysis

In the fibroblast cytotoxicity assay, after 24 h the CG cultures showed lower cell proliferation values compared with those of the groups cultured with 50% and 100% concentrations of biomaterial extract. Moreover, the group with 100% concentration of the extract presented significantly higher fibroblast proliferation values compared with the groups with 50%, 25% and 12.5% concentrations. After 72 and 144 h, no significant differences were found among all groups (Figure 6).

The osteoblast proliferation assay presented significant differences with the three different experimental periods: 24 h after seeding, the group with 100% concentration of extract showed a significantly higher value of osteoblast cell proliferation than did the CG and the 12.5% group; after 72 h a higher value of osteoblast proliferation in the 100% group was observed relative to the CG and 25% and 12.5% groups; finally, 144 h after seeding, the 100% group showed a higher value of osteoblast proliferation compared with all other biomaterial extract concentrations groups. For this same period, a higher value of osteoblast proliferation in the 50% group was observed relative to the 25% and 12.5% groups (Figure 7).

3.2.2. Genotoxicity analysis

The single-cell gel (comet) assay was performed to measure DNA damage in fibroblastic and osteoblastic cell

DOI: 10.1002/term

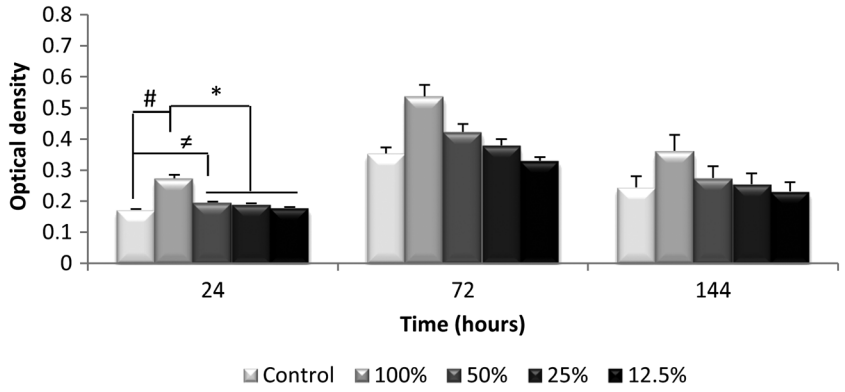

Figure 6. Proliferation of fibroblast cell line in solutions containing different concentrations of fibrous glassy scaffold extracts (100%, 50%, 25% and 12.5%) at different culture times (24, 72 and 144 h); $^{\#}p \leq 0.05$ vs CG; $^{\neq}p \leq 0.05$ vs CG; $^{*}p \leq 0.05$ vs 50%, 25% and 12.5%

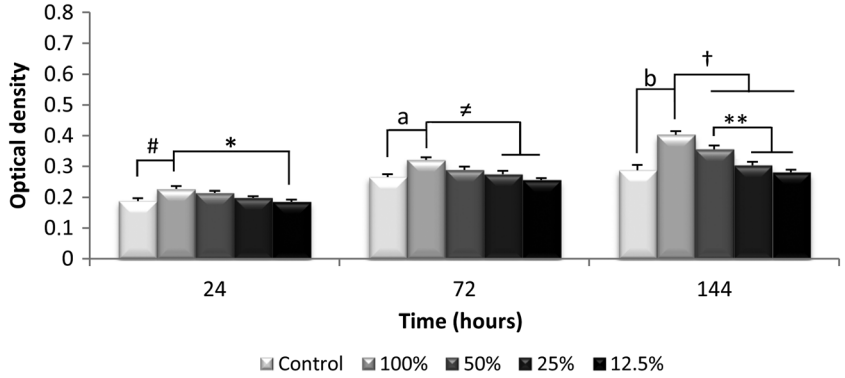

Figure 7. Proliferation of osteoblast cell line in solutions containing different concentrations of fibrous glassy scaffold extracts (100%, 50%, 25% and 12.5%) at different culture times (24, 72 and 144 h); $^{\#}p \leq 0.05$ vs CG; $^{*}p \leq 0.05$ vs 12.5%; $^{a}p \leq 0.05$ vs CG; $^{\neq}p \leq 0.05$ vs 25% and 12.5%; $^{b}p \leq 0.05$ vs CG; $^{\dagger}p \leq 0.05$ vs 50%, 25% and 12.5%; and $^{**}p \leq 0.05$ vs 25% and 12.5%

lines. There were no significant differences ($p > 0.05$) between the control and treated groups, indicating that the fibrous glassy scaffold did not induce DNA strand breaks in fibroblasts and osteoblasts for any evaluated period (Table 2).

3.3. *In vivo* results

3.3.1. General observation of the experimental animals

The animals showed no postoperative complications. They quickly returned to their normal diet and showed no loss of body mass. Furthermore, no animals died during the experiment and no infections in the injured areas were detected.

3.3.2. Histopathological analysis of subcutaneous implants

Fifteen days after implantation, clear signs of material degradation were observed (Figure 8A), with the presence of foreign body giant cells primarily around the fibres of the fibrous glassy scaffold. Granulation tissue was also noticed, with moderate inflammation in the degraded area of the implant. Moreover, a granulous capsule was observed around the implant (Figure 8B). At the biomaterial–tissue interface, a moderate number of inflammatory cells were observed.

After 30 days of implantation, the biomaterial degradation continued (Figure 8C). Many foreign body giant cells were observed, mainly around the fibres of the scaffold. Histological analyses revealed a greater amount of granulation tissue throughout the scaffold fibres compared with the previous period. Additionally, tissue ingrowth and inflammatory cells were noted in the voided spaces in the degraded biomaterial. Furthermore, a thinner mature fibrous capsule was observed, presenting fibroblasts and

Table 2. Mean and SE values of the tail moment (DNA damage) in fibroblast and osteoblast cells

	Experimental groups			
	Control*		Fibrous glassy scaffold	
Time (h)	Fibroblasts	Osteoblasts	Fibroblasts	Osteoblasts
24	0.8 + 0.4	0.7 + 0.3	1.0 + 0.4	0.6 + 0.2
72	0.5 + 0.2	1.1 + 0.5	0.7 + 0.2	1.3 + 0.5
144	0.4 + 0.3	0.8 + 0.2	0.5 + 0.4	0.8 + 0.4

*DMEM; $p > 0.05$.

DOI: 10.1002/term

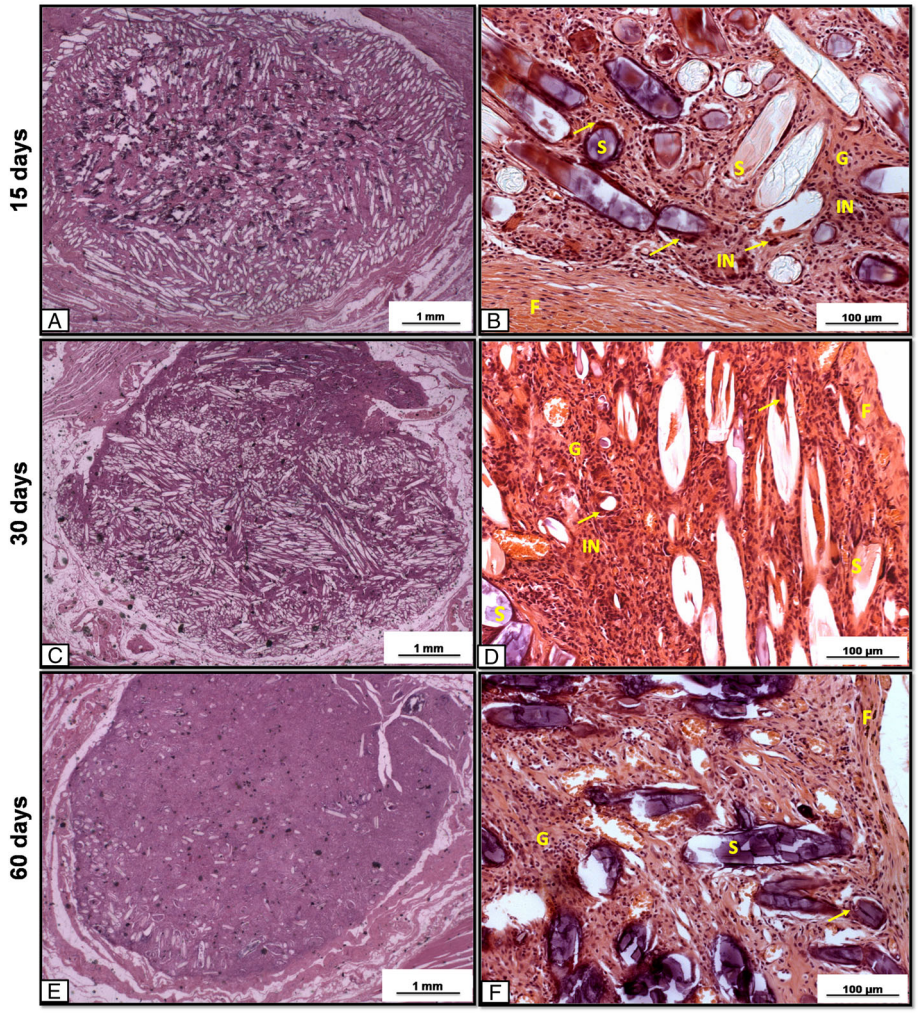

Figure 8. Representative histological subcutaneous implants of the three experimental periods: 15 (A, B); 30 (C, D); and 60 (E, F) days; magnification = ×12.5, bars = 1 mm; magnification = ×200, bars = 100 µm. IN, inflammatory cells; G, granulation tissue; S, fibres of the bioactive glassy scaffold; F, fibrous capsule; G, granulation tissue; and arrows, multinucleated giant cells; bar = 100 µm; H&E staining

inflammatory cells (Figure 8D). Directly adjacent to the surface of the implants (i.e. the interface), a moderate number of inflammatory cells were observed.

Implant degradation continued 60 days post-surgery to a larger extent compared with the other experimental periods (Figure 8E). Tissue ingrowth was observed in the degraded areas, with an organized granulation tissue resembling the connective tissue of the non-injured areas inside the implant. Some multinucleated giant cells were present around the fibres, although in some of the analysed samples no capsules were observed around the implants. The capsules, when present, had a thinner organized structure compared with the other periods (Figure 8F). At the biomaterial–tissue interface, the fibroblasts contacted the implant surface without the presence of macrophages or other inflammatory cells.

3.3.3. Quantitative histological evaluation of subcutaneous implants

The results from the histological quantitative analysis of the subcutaneous implants are shown in Figure 9. The capsules observed in the animals sacrificed on day 15 post-surgery were significantly thicker than those of the other groups (Figure 9A; $p < 0.05$). The quality of the capsule and the quality of the interface were also significantly different between the samples at 60 days and at the other two analysed periods (Figure 9B, C; $p < 0.05$).

4. Discussion

The present study evaluated the mineralization, physicochemical properties, degradation behaviour and biocompatibility of a fibrous glassy scaffold. The analysis demonstrated that the immersion of the scaffolds in SBF led to the formation of a crystallized HCA layer on the material surface in a short period of only 12 h. Moreover, an increased pH and an accelerated mass loss were also observed in the samples upon immersion in PBS. The *in vitro* study demonstrated increased fibroblast and osteoblast cell proliferations and no cell DNA damage after cell seeding. The subcutaneous implantation showed that

DOI: 10.1002/term

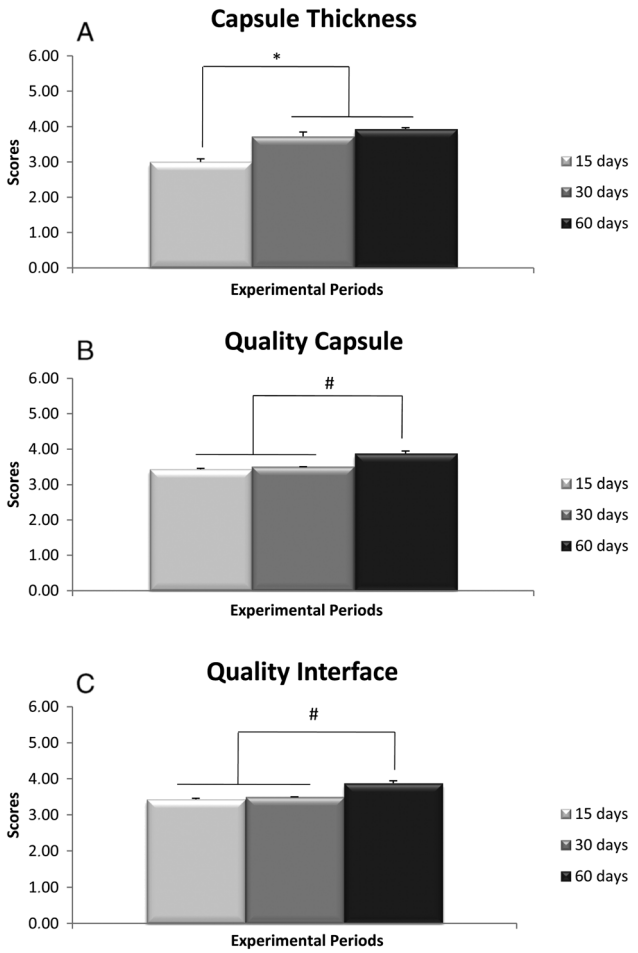

Figure 9. Histological evaluation of: (A) capsule thickness; (B) the quality of the capsule; and (C) the quality of the interface of the subcutaneous implants after 15, 30 and 60 days of implantation, using the histological grading scale. Error bars represent mean ± SE of the mean; $^{*}p < 0.05$ compared with 15 days; $^{\#}p < 0.05$ compared to with 15 and 30 days

the biomaterial indeed had a favourable effect on soft tissue responses in terms of capsule thickness, capsule quality and interface quality.

Bioactivity is one of the most desirable characteristics for a material to be used for bone tissue engineering (Hench *et al.,* 2004). The formation of the HCA layer observed in the FTIR evaluation indicates that this biomaterial possesses a very high *in vitro* bioactivity. Hence, it is possible to infer that, for this new glass composition, the rate of *in vitro* formation of the HCA layer, as assessed using the SBF test, is similar to that for Bioglass 45S5, which takes approximately 8 h for an HCA layer formation (Peitl *et al.,* 2001; Hench, 2006, 2013). The SEM image for the 16 h sample clearly shows the presence of the HCA layer, due to the easily detectable globular pattern of this crystalline phase. These data demonstrate that the porous fibrous glass composition is highly bioactive and reactive and is suitable for the fabrication of scaffolds and tissue-regeneration applications.

The pH measurements confirmed an alkalization of the immersion medium in the presence of the scaffold. The reactions at the sample interface were likely responsible for these observations. A release of ions (i.e. Si, Na, Ca and P) occurred immediately after the BG scaffolds contacted the fluids, resulting in an increased pH (Hench *et al.,* 2004; Day *et al.,* 2005). Moreover, the mass loss evaluation showed a significant decrease in mass 14 days after immersion, but the samples did not collapse. This behaviour may also be associated with the rapid ion release that is initiated immediately after the contact of BG with fluids, starting the degradation of the material (Kokubo *et al.,* 1990; Jones, 2013). Accordingly, Misra *et al.* (2010) and Bretcanu *et al.* (2014) also observed accelerated mass losses in a BG–poly(3-hydroxybutyrate) composite (approximately 15%) and in a resorbable phosphate glass scaffold (approximately 20%) after 14 days of immersion.

These leaching reactions (leading to ion release) are very common and well established for bioactive glasses and are defined by Hench as five-stage reactions (Hench, 2013). Briefly, in stage I, alkali and alkali earth ions are released from the glass into the fluid and are replaced by H^+ or H_3O^+ ions in the glass structure. This reaction increases the local pH, resulting in the rupture of Si–O–Si bonds. Then, in stage II, silicon is released into the fluid in the form of silanol groups ($Si(OH)_4$). In stage III, the silanols condense, forming a polymerized silica gel layer on the surface of the glass. Subsequently, in stage IV, calcium and phosphate ions that had diffused from the glass or from the fluid form an amorphous calcium phosphate layer over the silica gel. Following these reactions, in stage V, the amorphous calcium phosphate layer incorporates the carbonate species and crystallizes into HCA (Hench, 2013).

The indirect cytotoxicity assay showed that the biomaterial at 100% concentration of extract produced a significant increase in fibroblast proliferation 24 h after seeding. For the osteoblasts, increased proliferation rates were observed for all analysed set points, especially for the 100% group. The differences between the behaviours of the cell lines may be explained by their morphological shapes. Fibroblasts are flattened cells; it has been reported that this type of cell shows a higher proliferation rate than do round, spherical cells (Folkman and Moscona, 1978; Archer *et al.,* 1982; Wang *et al.,* 2003). Therefore, fibroblasts presented an earlier increased proliferation rate and earlier confluence compared with osteoblasts. The biomaterial degradation may have created a microenvironment that improved cellular activity and function. The cytotoxicity results demonstrated that the fibrous glassy scaffold did not present toxic potential. *In vitro* studies have demonstrated that different bioactive ceramics were also non-cytotoxic and were able to support significantly larger areas of *in vitro* calcified matrix in osteoblast cell cultures (Moura *et al.,* 2007), to support the attachment of human bone-derived cells (Radetzki *et al.,* 2011) and to stimulate the differentiation and proliferation of human osteoblastic-like cells (Wu *et al.,* 2010).

The single-cell gel (comet) assay detected no DNA damage for both tested cell lines, demonstrating that the fibrous glassy scaffold presented no genotoxic potential. From these results, it can be concluded that the dissolution

DOI: 10.1002/term

products from the fibrous glassy scaffold did not affect the DNA cells. Such data are in agreement with the results of a previous study conducted by Kido *et al.* (2013), who observed no DNA strand breaks in fibroblasts and osteoblasts cultured on Biosilicate® scaffolds after 24, 72 and 96 h. Likewise, Peláez *et al.* (2005) indicated no genotoxicity for ceramic coatings applied on stainless steel.

It is well known that biomaterial chemical features can affect tissue response and, consequently, modulate the foreign body reaction. Biomaterials may cause intense inflammatory responses and tissue irritation, which can culminate in delayed tissue healing (Anderson and McNally, 2011). In contrast, the histopathological analysis showed that the implantation of the fibrous glassy scaffold produced a discrete foreign body reaction, as evidenced by the presence of multinucleated giant cells around some fibres of the biomaterial in all experimental periods. The granulation tissue was also observed to gradually occupy the spaces left by the degraded biomaterial. In addition, at day 60, an organized granulation tissue (resembling the connective tissue of non-injured regions) in larger degraded areas and a thinner-organized capsule with a better interface were observed compared with the other periods. Furthermore, the tissue organization in the implantation area improved over time. It was likely that the degradation products of the material did not cause a severe tissue irritation; instead, the degraded material was bioabsorped (Akazawa *et al.,* 2006; Murata *et al.,* 2007) and, consequently, the injured tissue gradually reorganized over time.

Finally, the presence of interconnected pores is a key factor for tissue repair because it allows for the migration and proliferation of cells and promotes vascularization. Successful neovascularization results in higher oxygen supply and, consequently, in a readily available supply of nutrients for tissue repair (Taboas *et al.,* 2003; Karageorgiou and Kaplan, 2005; Rezwan *et al.,* 2006; Hoppe *et al.,* 2011; Baino and Vitale-Brovarone, 2014; Franca *et al.,* 2014; Yang *et al.,* 2014). The high porosity and interconnected porous structures of the fibrous glassy scaffold, as assessed in this study, may be relevant to the success of the biological performance of the fibrous glassy material.

Based on the *in vitro* and *in vivo* results of the tested fibrous glassy scaffolds, this investigation shows that the present biomaterial may be used as a bone graft for accelerating tissue repair. Further histomorphometric and immunohistochemical studies on this new biomaterial, regarding bone defect models, are necessary to evaluate its *in vivo* efficacy.

5. Conclusions

Highly porous, fibrous glassy scaffolds (using a new bioactive glass composition, F18) were developed, showing high bioactivity and mineralization in SBF-K9 solution in approximately 12 h. These new fibrous glassy scaffolds were biocompatible. Preliminary cytotoxicity data justify further biological studies to check how cells interact directly with the scaffolds. Taken together, these encouraging outcomes indicate the fibrous glassy scaffolds as promising materials for developing new types of therapeutic approaches related to health care and bone tissue engineering. However, additional long-term studies are required to fully investigate the behaviour of this new biomaterial for potential ortothopic *in vivo* applications.

Conflict of interest

The authors have declared that there is no conflict of interest.

Acknowledgements

The authors are indebted to CAPES, CNPq (Grant No. 303662/2012-3), FAPESP, the São Paulo Research Funding Agency, the Centre for Research Technology (Grant No. 2013/07793-6) and Education in Vitreous Materials (CeRTEV) for funding this research work. M.T.S. thanks FAPESP for student Grant No. 2011/22937-9.

Author contributions

Concept and design, P.R.G.A., M.T.S., P.S.B., O.P.F. and A. C.M.R.; acquisition of data, P.R.G.A., H.W.K., C.R.T., K.R. F., A.M.P.M. and D.A.R.; analysis and interpretation, P.R. G.A., H.W.K., C.R.T., P.S.B., K.R.F., D.A.R. and A.C.M.R.; drafting of manuscript, P.R.G.A., C.R.T., M.T.S., E.D.Z. and A.C.M.R.; critical revision of manuscript for important intellectual content, E.D.Z. and A.C.M.R.; statistical analyses, P.R.G.A., A.M.P.M. and A.C.M.R.; funding, P.R. G.A., M.T.S., N.A.P., K.P.S.F., R.A.M.F., E.D.Z. and A.C. M.R.; technical support, P.R.G.A., H.W.K., C.R.T., P.S.B., K.R.F., A.M.P.M., K.P.S.F. and R.A.M.F.; and study supervision, O.P.F. and A.C.M.R.

References

Akazawa T, Murata M, Sasaki T *et al.* 2006; Biodegradation and bioabsorption innovation of the functionally graded bovine bone-originated apatite with blood permeability. *J Biomed Mater Res A* **76**: 44–51.

Anderson JM, McNally AK. 2011; Biocompatibility of implants: lymphocyte/macrophage interactions. *Semin Immunopathol* **33**: 221–233.

Archer CW, Rooney P, Wolpert L. 1982; Cell shape and cartilage differentiation of early chick limb bud cells in culture. *Cell Differ* **11**: 245–251.

Baino F, Vitale-Brovarone C. 2014; Mechanical properties and reliability of glass–ceramic foam scaffolds for bone repair. *Mater Lett* **118**: 27–30.

Bretcanu O, Baino F, Verne E *et al.* 2014; Novel resorbable glass–ceramic scaffolds for hard tissue engineering: from the parent phosphate glass to its bone-like macroporous derivatives. *J Biomater Appl* **28**: 1287–1303.

Brown RF, Day DE, Day TE *et al.* 2008; Growth and differentiation of osteoblastic cells on 13–93 bioactive glass fibers and scaffolds. *Acta Biomater* **4**: 387–396.

Chen QZ, Thompson ID, Boccaccini AR. 2006; 45S5 Bioglass-derived glass–ceramic scaffolds for bone tissue engineering. *Biomaterials* **27**: 2414–2425.

Claes L, Willie B. 2007; The enhancement of bone regeneration by ultrasound. *Prog Biophys Mol Biol* **93**: 384–398.

Day RM, Maquet V, Boccaccini AR *et al.* 2005; *In vitro* and *in vivo* analysis of macroporous biodegradable poly(D,L-lactide-co-glycolide) scaffolds containing bioactive glass. *J Biomed Mater Res A* **75**: 778–787.

Folkman J, Moscona A. 1978; Role of cell shape in growth control. *Nature* **273**: 345–349.

Franca R, Samani TD, Bayade G *et al.* 2014; Nanoscale surface characterization of biphasic calcium phosphate, with comparisons to calcium hydroxyapatite and *β*-tricalcium phosphate bioceramics. *J Colloid Interface Sci* **420**: 182–188.

Gautier E, Sommer C. 2003; Guidelines for the clinical application of the LCP. *Injury* **34**(suppl 2): B63–76.

Ghasemi-Mobarakeh L, Semnani D, Morshed M. 2007; A novel method for porosity measurement of various surface layers of nanofibers mat using image analysis for tissue engineering applications. *J Appl Polym Sci* **106**: 2536–2542.

Gorustovich AA, Roether JA, Boccaccini AR. 2010; Effect of bioactive glasses on angiogenesis: a review of *in vitro* and *in vivo* evidence. *Tissue Eng B Rev* **16**: 199–207.

Granito RN, Renno AC, Ravagnani C *et al.* 2011; *In vivo* biological performance of a novel, highly bioactive glass–ceramic (Biosilicate®): a biomechanical and histomorphometric study in rat tibial defects. *J Biomed Mater Res B Appl Biomater* **97**: 139–147.

Hench LL. 2006; The story of bioglass. *J Mater Sci Mater Med* **17**: 967–978.

Hench LL. 2013; Introduction to Bioceramics, 2nd edn. Imperial College Press: London; 620. ISBN: 978–1-908977–15–1.

Hench LL, Polak JM. 2002; Third-generation biomedical materials. *Science* **295**: 1014–1017.

Hench LL, Xynos ID, Polak JM. 2004; Bioactive glasses for *in situ* tissue regeneration. *J Biomater Sci Polym Ed* **15**: 543–562.

Hoppe A, Guldal NS, Boccaccini AR. 2011; A review of the biological response to ionic dissolution products from bioactive glasses and glass–ceramics. *Biomaterials* **32**: 2757–2774.

Hubbell JA. 1998; Synthetic biodegradable polymers for tissue engineering and drug delivery. *Curr Opin Solid State Mater Sci* **3**: 4.

ISO IOFS. 2003; Biological evaluation of medical devices, part 3: tests for genotoxicity, carcinogenicity and reproductive toxicity; 10993–3. ISO: Geneva.

Jansen JA, Dhert WJ, Van Der Waerden JP *et al.* 1994; Semi-quantitative and qualitative histologic analysis method for the evaluation of implant biocompatibility. *J Invest Surg* **7**: 123–134.

Jones JR. 2013; Review of bioactive glass: from Hench to hybrids. *Acta Biomater* **9**: 4457–4486.

Karageorgiou V, Kaplan D. 2005; Porosity of 3D biomaterial scaffolds and osteogenesis. *Biomaterials* **26**: 5474–5491.

Kido HW, Oliveira P, Parizotto NA *et al.* 2013; Histopathological, cytotoxicity and genotoxicity evaluation of Biosilicate® glass–ceramic scaffolds. *J Biomed Mater Res A* **101**: 667–673.

Kokubo T, Kushitani H, Sakka S *et al.* 1990; Solutions able to reproduce *in vivo* surface-structure changes in bioactive glass–ceramic A-W. *J Biomed Mater Res* **24**: 721–734.

Lacroix J, Jallot E, Lao J. 2014; Gelatin-bioactive glass composites scaffolds with controlled macroporosity. *Chem Eng J* **256**: 9–13.

Link DP, Van Den Dolder J, Van Den Beucken JJ *et al.* 2008; Evaluation of the biocompatibility of calcium phosphate cement/PLGA microparticle composites. *J Biomed Mater Res A* **87**: 760–769.

Liu W, Chang J. 2012; Setting properties and biocompatibility of dicalcium silicate with varying additions of tricalcium aluminate. *J Biomater Appl* **27**: 171–178.

Liu X, Huang W, Fu H *et al.* 2009; Bioactive borosilicate glass scaffolds: *in vitro* degradation and bioactivity behaviors. *J Mater Sci Mater Med* **20**: 1237–1243.

Mirhadi SM. 2014; Synthesis and characterization of nanostructured forsterite scaffolds using two step sintering method. *J Alloys Compounds* **610**: 399–401.

Misra SK, Ansari T, Mohn D *et al.* 2010; Effect of nanoparticulate bioactive glass particles on bioactivity and cytocompatibility of poly(3-hydroxybutyrate) composites. *J R Soc Interface* **7**: 453–465.

Moimas L, Biasotto M, Di Lenarda R *et al.* 2006; Rabbit pilot study on the resorbability of three-dimensional bioactive glass fibre scaffolds. *Acta Biomater* **2**: 191–199.

Mosmann T. 1983; Rapid colorimetric assay for cellular growth and survival: application to proliferation and cytotoxicity assays. *J Immunol Methods* **65**: 55–63.

Moura J, Teixeira LN, Ravagnani C *et al.* 2007; *In vitro* osteogenesis on a highly bioactive glass–ceramic (biosilicate). *J Biomed Mater Res A* **82**: 545–557.

Murata M, Akazawa T, Tazaki J *et al.* 2007; Blood permeability of a novel ceramic scaffold for bone morphogenetic protein-2. *J Biomed Mater Res B Appl Biomater* **81**: 469–475.

Naghavi N, Ghoddusi J, Sadeghnia HR *et al.* 2014; Genotoxicity and cytotoxicity of mineral trioxide aggregate and calcium enriched mixture cements on L929 mouse fibroblast cells. *Dent Mater J* **33**: 64–69.

Narayan R. 2009; Scanning Electron Microscopy Combined with Image Analysis Software Can also be Used to Estimate Porosity, Pore size and Distribution. Springer: Chapel Hill, NC, USA.

Nath S, Kalmodia S, Basu B. 2010; Densification, phase stability and *in vitro* biocompatibility property of hydroxyapatite–10 wt% silver composites. *J Mater Sci Mater Med* **21**: 1273–1287.

Peitl O, Dutra Zanotto E, Hench LL. 2001; Highly bioactive P_2O_5–Na_2O–CaO–SiO_2 glass–ceramics. *J Non-crystal Solids* **292**: 115–126.

Peláez A, García CP, Pareja A *et al.* 2005; Genotoxicity effects of ceramic coatings applied on metallic substrates using single cell gel electrophoresis assay. *In vitro Key Eng Mater* **284**(86): 593–596.

Radetzki F, Wohlrab D, Zeh A *et al.* 2011; Cellular compatibility of highly degradable bioactive ceramics for coating of metal implants. *Biomed Mater Eng* **21**: 307–321.

Rahaman MN, Day DE, Bal BS *et al.* 2011; Bioactive glass in tissue engineering. *Acta Biomater* **7**: 2355–2373.

Renno AC, Van De Watering FC, Nejadnik MR *et al.* 2013; Incorporation of bioactive glass in calcium phosphate cement: an evaluation. *Acta Biomater* **9**: 5728–5739.

Rezwan K, Chen QZ, Blaker JJ *et al.* 2006; Biodegradable and bioactive porous polymer/inorganic composite scaffolds for bone tissue engineering. *Biomaterials* **27**: 3413–3431.

Serrano MC, Portoles M, Pagani R *et al.* 2008; *In vitro* positive biocompatibility evaluation of glass–glass ceramic thermoseeds for hyperthermic treatment of bone tumors. *Tissue Eng A* **14**: 617–627.

Souza MT, Zanotto ED, Peitl-Filho O. 2013; Vitreous composition, bioactive glassy fibers and tissues. Patent Application No. BR 10 2013 020961 9; Universidade Federal de São Carlos, Brazil, Patent Application No. BR 10 2013 020961 9.

Taboas JM, Maddox RD, Krebsbach PH *et al.* 2003; Indirect solid free-form fabrication of local and global porous, biomimetic and composite 3D polymer–ceramic scaffolds. *Biomaterials* **24**: 181–194.

Tice RR, Agurell E, Anderson D *et al.* 2000; Single cell gel/comet assay: guidelines for *in vitro* and *in vivo* genetic toxicology testing. *Environ Mol Mutagen* **35**: 206–221.

Vallet-Regi M. 2006; Revisiting ceramics for medical applications. *Dalton Trans* **44**: 5211–5220.

Wang XH, Zhu Y, Feng QL *et al.* 2003; Responses of osteo- and fibroblast cells to phosphorylated chitin. *J Bioact Compat Polym* **18**: 135–146.

Wu C, Ramaswamy Y, Zreiqat H. 2010; Porous diopside ($CaMgSi_2$)O_6 scaffold: a promising bioactive material for bone tissue engineering. *Acta Biomater* **6**: 2237–2245.

Xie ZP, Zhang CQ, Yi CQ *et al.* 2009; *In vivo* study effect of particulate bioglass in the prevention of infection in open fracture fixation. *J Biomed Mater Res B Appl Biomater* **90**: 195–201.

Xynos ID, Edgar AJ, Buttery LD *et al.* 2000; Ionic products of bioactive glass dissolution increase proliferation of human osteoblasts and induce insulin-like growth factor II mRNA expression and protein synthesis. *Biochem Biophys Res Commun* **276**: 461–465.

Yang JZ, Sultana R, Hu XZ *et al.* 2014; Novel layered hydroxyapatite–tri-calcium phosphate–zirconia scaffold composite with high bending strength for load-bearing bone implant application. *Int J Appl Ceram Technol* **11**: 22–30.

DOI: 10.1002/term